Fine-structure spectrum of the FO radical, observed by far-infrared laser magnetic resonance

Filippo Tamassia and John M. Brown[a)]
Physical and Theoretical Chemistry Laboratory, South Parks Road, Oxford OX1 3QZ, United Kingdom

Kenneth M. Evenson
National Institute of Standards and Technology, 325 Broadway, Boulder, Colorado 80303

(Received 1 December 1998; accepted 20 January 1999)

The fine-structure transition $^2\Pi_{1/2}\leftarrow{}^2\Pi_{3/2}$ of the free radical FO has been detected by far-infrared laser magnetic resonance. All the observed transitions are magnetic dipole in character. The spin–orbit constant A_0 has been determined experimentally; its value of $-196.108\,686(50)$ cm^{-1} is consistent with previous estimates. The analysis of a set of 290 transitions leads to the determination of a number of molecular parameters including rotational, centrifugal distortion, spin–orbit, lambda-doubling, magnetic hyperfine, and Zeeman terms. All four magnetic hyperfine structure constants a, b_F, c, d for the ^{19}F nucleus have been determined and are discussed in terms of the expectation values of the appropriate operators over the electronic wave function. © *1999 American Institute of Physics.* [S0021-9606(99)01315-X]

INTRODUCTION

The first experimental detection of the FO radical was made by McKellar[1] in 1979 through the observation of its infrared spectrum. He recorded the fundamental vibration–rotation band associated with the lower spin component $^2\Pi_{3/2}$ by CO_2-laser magnetic resonance (LMR) spectroscopy and determined the band origin ν_0, the rotational constant B_0, the centrifugal distortion correction D_0, the hyperfine parameter $h_{3/2}=a+\frac{1}{2}(b+c)$, the vibrational differences B_1-B_0, h_1-h_0, and the spin–orbit constant A_0. Since the observations were confined to the $\Omega=3/2$ spin component, A_0 could not be determined directly, and in fact the reported value of $-177.3(57)$ cm^{-1} was not very accurate. Subsequently, the same vibrational band was reinvestigated by diode laser spectroscopy,[2] leading to a better determination of B_0, B_1, D_0, D_1 because it was now possible to study FO in both spin components.

Burkholder *et al.*[3] recorded the 1–0 and 2–0 bands in both $^2\Pi_{3/2}$ and $^2\Pi_{1/2}$ spin components by Fourier transform IR spectroscopy. In 1988 the same infrared bands and a number of $\Delta v=1,2,3$ bands were recorded in a Fourier transform emission experiment by Hammer *et al.*[4] The set of reported data was fitted to an effective Hamiltonian which included rotational, centrifugal distortion, spin–orbit, and lambda-doubling terms. Nuclear hyperfine structure was not resolved. A_0 was estimated to be $-198.3(67)$ cm^{-1} in Ref. 3 and $-193.28(97)$ cm^{-1} in Ref. 4, still indirectly and subject to quite a large uncertainty. As pointed out by the authors of Ref. 4, the comparison of all the available experimental determinations and theoretical calculations suggested that A_0 could lie between -180 and -200 cm^{-1}; that is to say, a major parameter of FO was still very poorly determined.

The best way to measure the spin–orbit splitting is the direct detection of the fine-structure transition $^2\Pi_{1/2}\leftarrow{}^2\Pi_{3/2}$ in the far-infrared region. This is the aim of the present work. The LMR technique was chosen because of its high sensitivity and its ability to discriminate between open-shell and closed-shell molecules, which are usually present in much higher amounts; also, the only intense sources in the far-infrared (FIR) region are fixed-frequency lasers. In a Hund's case (a) limit, the fine-structure transition is electric dipole forbidden but magnetic dipole allowed and hence it is expected to be three or four orders of magnitude weaker than a normal, electric dipole allowed transition. On the other hand, Brown, Cole, and Honey,[5] in their work on the fine-structure spectrum of NO, pointed out that magnetic dipole allowed transitions were about 18 times stronger than electric dipole forbidden transitions. The same ratio is 20 for SeH[6] and 140 for BrO;[7] it depends on the magnitude of the electric dipole moment and the spin–orbit splitting.

Burkholder *et al.*[3] have also considered the production of FO by the reaction between F atoms and ozone and emphasized that, in the presence of excess ozone, there is no net loss of FO radicals. FO is produced by the reaction

$$F+O_3\rightarrow FO+O_2 \tag{1}$$

and destroyed by the reaction

$$FO+FO\rightarrow 2F+O_2. \tag{2}$$

Thus two F atoms are produced in the latter process and can react with further ozone molecules, thereby regenerating the FO radical. This was confirmed in our experiments where we observed a surprisingly long lifetime of the signal (see the experimental section). These considerations and the high intrinsic sensitivity of LMR gave us confidence in our approach to the experiment, despite the expected low intensity of the magnetic dipole transitions.

No pure rotational or electron paramagnetic resonance spectra of FO have been reported in the literature. McKellar[8]

a)Electronic mail: jmb@physchem.ox.ac.uk

combined LMR spectroscopy and Stark spectroscopy to demonstrate that the electric dipole moment of FO is 0.0043(4) D for the $v=0$ level and 0.0267(9) D for $v=1$. The exceptionally small value of μ has therefore precluded any detection of rotational spectra so far but the strong variation of μ with the vibrational excitation makes the infrared spectra relatively easy to observe. This is supported by theoretical calculations by Langhoff, Bauschlicher, and Partridge.[9] Their predictions for $\mu_{v=0}$ (-0.0089 D with the negative end on the F atom) and $\mu_{v=1}$ (-0.0318 D) show quite good agreement with McKellar's experimental values. The computed curve of the dipole moment as a function of the internuclear distance shows a steep slope for bond lengths less than 0.16 nm, confirming the large change of μ passing from $v=0$ to $v=1$.

In the present paper, we report the successful detection of magnetic dipole, fine-structure transitions of the FO radical in the $v=0$ level of the $X\,^2\Pi$ state. The measurements are more accurate than any which precede it and allow, among other things, the first direct determination of the spin–orbit coupling constant and of all four magnetic nuclear hyperfine parameters.

EXPERIMENTAL DETAILS

The far-infrared spectrometer used for the experiment has been described elsewhere.[10] Very recently[11] some changes have been made: the Zeeman modulation frequency has been raised to 40 kHz to improve the sensitivity and the diameter of the pump tube has been reduced in order to produce better performance of the laser at wavelengths shorter than 100 μm. This has been proved to be particularly important for our experiment since the fine structure transitions of FO are around 50 μm. The detector used was a liquid-helium-cooled gallium–germanium photoconductor.

FO was produced by reacting F atoms with O_3. The F atoms were generated by flowing a 10% F_2 in He mixture through a microwave discharge. Ozone was introduced into the cell by flowing He over silica gel, on which ozone was adsorbed. The O_3/silica gel trap was placed in an ethanol–dry ice bath to regulate the amount of O_3 evaporated. The best signals were observed with 24 Pa (180 mTorr) of F_2/He and 9.3 Pa (70 mTorr) of O_3/He. As described in the Introduction, the production of FO was sustained by an excess of O_3, even in the absence of further F atoms. The interesting result is that, if the microwave discharge is switched off and the flow of ozone is maintained, the signal is maintained for a few minutes. This is not due to a very long lifetime of FO but to the regeneration of fluorine atoms by the reaction of two FO molecules. Signals of lower intensity were also observed reacting F atoms (42.7 Pa 10% F_2/He) with O_2 (100 Pa).

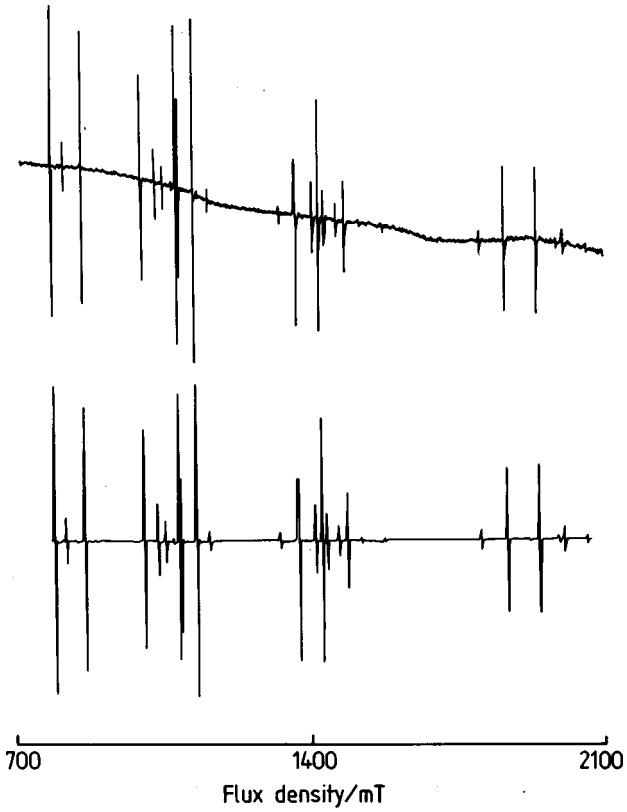

FIG. 1. Experimental (the upper trace) and simulated (the lower trace) far-infrared laser magnetic resonance spectrum of the $R(4\frac{1}{2})$ fine-structure transition of FO observed at 209.819 231 cm^{-1} in perpendicular polarization ($\Delta M_J=\pm 1$).

The spectra were recorded on an *xy* plotter as a function of the magnetic flux density. Since $1-f$ detection with magnetic modulation was employed, the first derivative of the absorption profile was observed. Figure 1 shows a long sur-

TABLE I. FIR laser lines used to record LMR spectra for FO.

CO_2 laser line[a]	Laser gas	Wavelength/μm	Frequency/MHz	Assigned FO transitions
$10R(46)$	CH_3OH	52.004	5 764 826.7	$P(2\frac{1}{2})$
$10R(56)$	CD_3OH	51.478	5 823 660.9*	$P(1\frac{1}{2})$
$10R(20)$	CD_3OH	50.629	5 921 370.4*	$Q(1\frac{1}{2})$, $Q(2\frac{1}{2})$
$10R(24)$	CD_3OH	49.973	5 999 028.8*	$Q(11\frac{1}{2})$, $Q(12\frac{1}{2})$, $Q(13\frac{1}{2})$, $Q(14\frac{1}{2})$
$10R(52)$	CH_3OH	49.694	6 032 811.3*	$Q(15\frac{1}{2})$, $Q(16\frac{1}{2})$, $Q(17\frac{1}{2})$
$9P(12)$	$^{13}CH_3OH$	49.455	6 061 914.8*	$Q(17\frac{1}{2})$, $Q(18\frac{1}{2})$, $Q(19\frac{1}{2})$, $Q(20\frac{1}{2})$
$9R(6)$	CD_3OH	48.721	6 153 279.0*	$R(2\frac{1}{2})$
$9R(8)$	CH_3OD	47.660	6 290 222.3*	$R(4\frac{1}{2})$
$9P(10)$	CH_3OH	46.165	6 493 911.5	$R(7\frac{1}{2})$

[a]Reference 28. The lines marked with an asterisk have been frequency measured for this work.

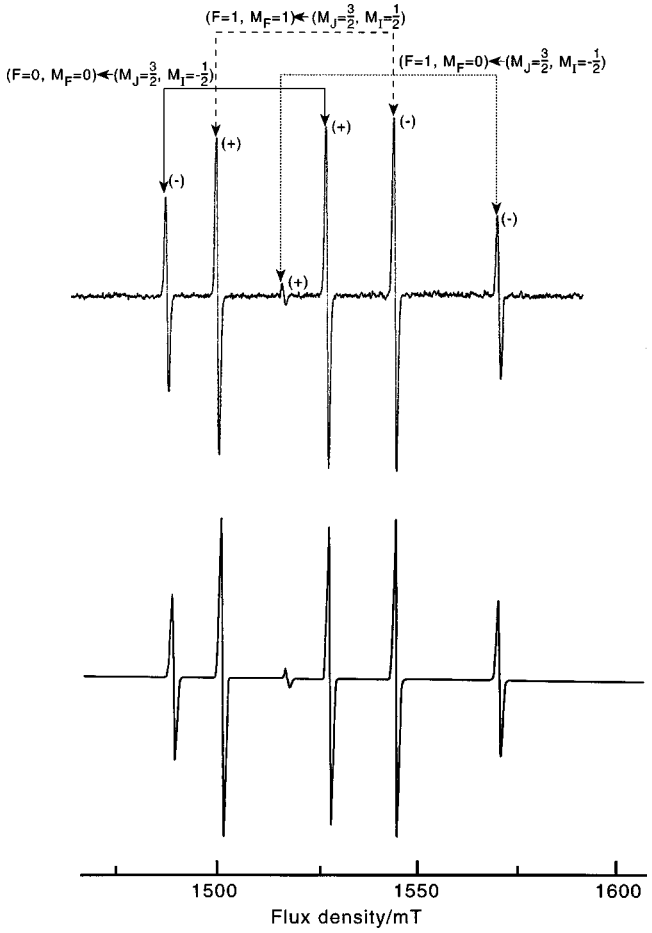

FIG. 2. Experimental (the upper trace) and simulated (the lower trace) far-infrared laser magnetic resonance spectrum of the $P(1\frac{1}{2})$ fine-structure transition of FO observed at 194.256 417 cm^{-1} in perpendicular polarization ($\Delta M_J = \pm 1$). Note the complicated hyperfine structure because of the difference in coupling schemes in the lower and upper states.

vey scan of the $R(4\frac{1}{2})$ transition. The spectra have been recorded in both parallel ($B_\omega \| B_0$) and perpendicular ($B_\omega \perp B_0$) polarizations. Typical measurement scans covered 40 mT and were performed back and forth to correct shifts due to the time constant. The magnet was periodically calibrated with a NMR gaussmeter: the overall fractional uncertainty is $\pm 1\times10^{-4}$ above 0.1 T and $\pm 1\times10^{-5}$ below 0.1 T. We estimate an experimental uncertainty of $\pm 2\times10^{-4}$ T for an individual resonance.

We used nine FIR laser lines to make our observations (see Table I) and seven of their frequencies have been measured for the first time in this experiment. Their frequency was determined by measuring the beat frequency when the FIR radiation was mixed with the radiation from two frequency-stabilized CO_2 lasers in a metal–insulator–metal (MIM) diode.[12]

RESULTS AND ANALYSIS

Nine laser lines, listed in Table I, have been used to record all of the spectra reported in this paper. The total range explored is about 24 cm^{-1} and covers part of the *P*, *Q*, and *R* branches of the fine-structure transition. Examples of typical spectra are shown in Figs. 1–3. We have recorded and assigned 290 lines corresponding to 17 rotational transitions with *J* ranging from $\frac{1}{2}$ to $20\frac{1}{2}$. All the observed resonances are magnetic dipole in origin. The spectrum of the $(J=18\frac{1}{2},\ F=19,\ M_F=-19,-)\leftarrow(J=18\frac{1}{2},\ M_I=-\frac{1}{2}, M_J=-\frac{39}{2},-)$ transition showed a Lamb dip, at low pressure and modulation amplitude, which indicates that the signals are strong enough to reach saturation and also that there is no underlying structure in the Doppler profile (see Fig. 4). No evidence for FO in vibrationally excited states has been found and all of the recorded lines have been assigned to fine-structure transitions in $v=0$.

By comparison of our spectra with the LMR spectra reported by Mizushima, Evenson, and Wells[13] in their work on the corresponding fine-structure transition of NO, we identified the different *Q* branches of our spectrum and obtained a rough idea of the value of *J*. Using the parameters of FO already known from literature[3,4] and hyperfine constants scaled from the corresponding parameters of CF,[14] the high-*J* *Q* branch was tentatively assigned. A_0 was changed step by step in order to match the calculated pattern with the experimental pattern. Once the first transition was identified, the spectroscopic constants were refined and new predictions made. The analysis of the spectra was lengthy and elaborate because of our ignorance of some basic parameters and the unusual Zeeman patterns,[7] which arise from the different nuclear spin coupling schemes in the upper and lower levels.

For a molecule in a $^2\Pi$ state there are two possible values, 3/2 and 1/2, for magnitude of the projection Ω of the angular momentum **J** on the internuclear axis. The two spin components, $^2\Pi_{3/2}$ and $^2\Pi_{1/2}$, show very different behavior in the presence of an external magnetic field. For a molecule which conforms closely to Hund's case (a) coupling, such as FO ($A_0 \simeq -196\ cm^{-1}$, $B_0 \simeq 1\ cm^{-1}$) the first-order Zeeman contribution to the total energy is given by

$$E_{\mathrm{Zee}} = g_J \mu_B B M_J, \tag{3}$$

where g_J is the *g* factor for the rotational level *J*, μ_B is the Bohr magneton, *B* is the magnetic flux density, and M_J is the projection of **J** on the laboratory-fixed *Z* axis. The *g* factor is given by

$$g_J = \frac{(\Lambda+\Sigma)(\Lambda+g_S\Sigma)}{J(J+1)}, \tag{4}$$

where Λ and Σ are, respectively, the projections of **L** and **S** on the internuclear axis. According to Eq. (4) g_J is nearly zero for the $^2\Pi_{1/2}$ state, while it is nonvanishing for the $^2\Pi_{3/2}$ state; in other words, the $^2\Pi_{1/2}$ state is essentially diamagnetic. As a result, the energy level patterns for the two types of state in a magnetic field are considerably different. In Fig. 5 the energy level diagram for the $P(1\frac{1}{2})$ transition at a flux density of 1.5 T is given.

For the lower state ($J=3/2$) the interaction with a magnetic field produces four M_J components, 3/2, 1/2, −1/2, −3/2, spread over 1.7 cm^{-1}. Each M_J level is in turn split into two levels by magnetic hyperfine interaction ($I_F=1/2$) and a further two by lambda-doubling effects. The finer splittings between these four sublevels cannot be appreciated on

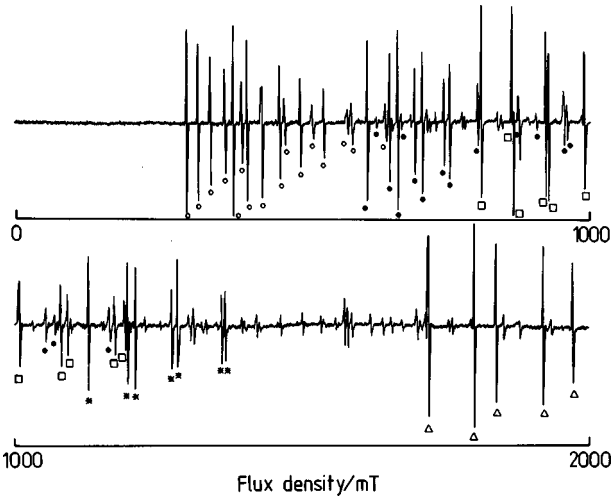

FIG. 3. Experimental far-infrared laser magnetic resonance spectrum of the $Q(15\frac{1}{2})$, $Q(16\frac{1}{2})$, $Q(17\frac{1}{2})$ transitions of FO observed at 201.232 924 cm^{-1} in parallel polarization ($\Delta M_J=0$). The measured lines are identified as follows: □—$Q(15\frac{1}{2})_+$, △—$Q(15\frac{1}{2})_-$, ○—$Q(16\frac{1}{2})_+$, ●—$Q(16\frac{1}{2})_-$, *—$Q(17\frac{1}{2})_-$.

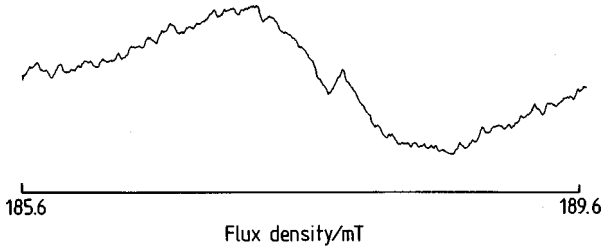

FIG. 4. A spectrum of the ($J=18\frac{1}{2}$, $F=19$, $M_F=-19,-$)←($J=18\frac{1}{2}$, $M_I=-\frac{1}{2}$, $M_J=-\frac{39}{2},-$) transition of FO observed at 202.203 713 cm^{-1} in parallel polarization ($\Delta M_J=0$) showing a single Lamb dip. Total pressure 22 Pa (165 mTorr), scan time 5 min, time constant 1 s, sensitivity 100 μV, modulation 0.1 mT.

the scale of the diagram, being much smaller than the separation between the M_J components. In this situation the nuclear spin **I** is decoupled from **J** so that J, M_J, I, M_I and the parity are all good quantum numbers. For the upper $J=1/2$ state in the same field, the Zeeman levels are spread over a much narrower range of energy (0.036 cm^{-1}) and there is no clear magnetic structure. In this case the nuclear spin remains coupled and only F ($\mathbf{F}=\mathbf{J}+\mathbf{I}$), its projection on the field axis M_F and the parity are good quantum numbers. The $J=1/2$ eigenfunctions in the coupled representation can be expressed as a linear combination of the decoupled basis set $|JM_JIM_I\rangle$ and, in the specific case of the $P(1\frac{1}{2})$ transition in FO they are, neglecting J and I:

$$|F=1,M_F=-1,-\rangle=|M_J=-\tfrac{1}{2},M_I=-\tfrac{1}{2},-\rangle,$$

$$|F=1,M_F=0,-\rangle=0.735|M_J=-\tfrac{1}{2},M_I=\tfrac{1}{2},-\rangle + 0.677|M_J=\tfrac{1}{2},M_I=-\tfrac{1}{2},-\rangle,$$

$$|F=1,M_F=1,-\rangle=|M_J=\tfrac{1}{2},M_I=\tfrac{1}{2},-\rangle,$$

$$|F=1,M_F=0,+\rangle=0.609|M_J=-\tfrac{1}{2},M_I=\tfrac{1}{2},+\rangle + 0.792|M_J=\tfrac{1}{2},M_I=-\tfrac{1}{2},+\rangle,$$

$$|F=1,M_F=1,+\rangle=|M_J=\tfrac{1}{2},M_I=\tfrac{1}{2},+\rangle,$$

$$|F=1,M_F=-1,+\rangle=|M_J=-\tfrac{1}{2},M_I=-\tfrac{1}{2},+\rangle,$$

$$|F=0,M_F=0,-\rangle=-0.677|M_J=-\tfrac{1}{2},M_I=\tfrac{1}{2},-\rangle + 0.735|M_J=\tfrac{1}{2},M_I=-\tfrac{1}{2},-\rangle,$$

$$|F=0,M_F=0,+\rangle=-0.792|M_J=-\tfrac{1}{2},M_I=\tfrac{1}{2},+\rangle + 0.609|M_J=\tfrac{1}{2},M_I=-\tfrac{1}{2},+\rangle,$$

where the calculations have been made for a flux density of 1.5 T and use the molecular parameters in Table III. The

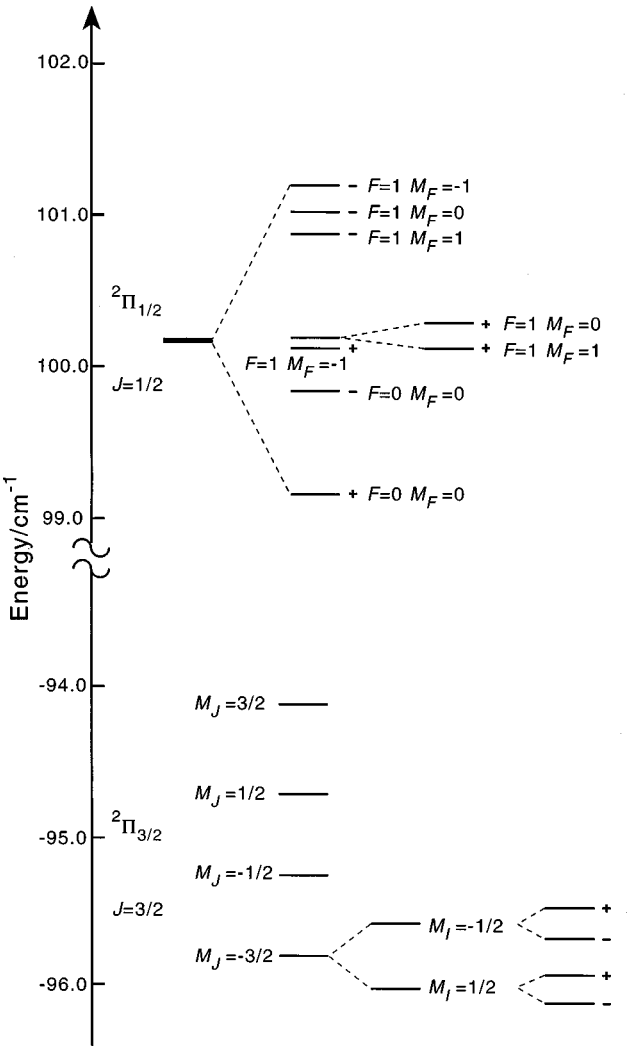

FIG. 5. Energy level diagram for the $P(1\frac{1}{2})$ fine-structure transition of FO calculated in a flux density of 1.5 T. For the $^2\Pi_{3/2}$ component, the fluorine nuclear spin is decoupled and every M_J level is split into two levels by the nuclear hyperfine interaction, each of which is further split by the effect of lambda doubling. The four energy levels associated with each single M_J component are not visible on the present scale; an enlargement is shown for $M_J=-3/2$. For the $^2\Pi_{1/2}$ component, the nuclear spin remains coupled to the overall rotational angular momentum **J**; the quantum numbers F and M_F are therefore appropriate. The energy levels in the $^2\Pi_{1/2}$ component have been expanded, since their separation is not visible on the present scale. Note that the levels ($F=1$, $M_F=0$, +) and ($F=1$, $M_F=1$, +) are overlapped.

$P(1\frac{1}{2})$ transition is shown in Fig. 2, where the simulated spectrum is also given. The six peaks correspond to the transitions:

(i) $|F=0,M_F=0,-\rangle \leftarrow |M_J=\frac{3}{2},M_I=-\frac{1}{2},-\rangle$,
$B_0=1489.17$ mT,

(ii) $|F=1,M_F=1,+\rangle \leftarrow |M_J=\frac{3}{2},M_I=\frac{1}{2},+\rangle$,
$B_0=1501.60$ mT,

(iii) $|F=1,M_F=0,+\rangle \leftarrow |M_J=\frac{3}{2},M_I=-\frac{1}{2},+\rangle$,
not measured,

(iv) $|F=0,M_F=0,+\rangle \leftarrow |M_J=\frac{3}{2},M_I=-\frac{1}{2},+\rangle$,
$B_0=1528.97$ mT,

(v) $|F=1,M_F=1,-\rangle \leftarrow |M_J=\frac{3}{2},M_I=\frac{1}{2},-\rangle$,
$B_0=1545.84$ mT,

(vi) $|F=1,M_F=0,-\rangle \leftarrow |M_J=\frac{3}{2},M_I=-\frac{1}{2},-\rangle$,
$B_0=1571.73$ mT.

Transitions (i), (iii), (iv) and (vi) involve heavily mixed basis functions and are in part forbidden because of the decoupled selection rule $\Delta M_I=0$.

As mentioned before, we cannot analyze the data in terms of a single coupling scheme. We chose to calculate the eigenvalues for the two spin components in the most appropriate basis sets, that is **I**-decoupled $|\eta\Lambda\rangle|S\Sigma\rangle|JM_J\Omega\rangle|IM_I\rangle$ for $^2\Pi_{3/2}$ and **I**-coupled $|\eta\Lambda\rangle|S\Sigma\rangle|JIFM_F\rangle$ for $^2\Pi_{1/2}$. The set of data has been fitted with an effective Hamiltonian[15,16] of the form

$$H_{\rm eff}=H_{\rm so}+H_{\rm rot}+H_{\rm cd}+H_{\rm LD}+H_{\rm cdLD}+H_{\rm hfs}+H_Z, \tag{5}$$

where

$$H_{\rm so}=A_0L_zS_z+\tfrac{1}{2}A_D[\mathbf{N}^2,L_zS_z]_+, \tag{6}$$

$$H_{\rm rot}=B_0\mathbf{N}^2, \tag{7}$$

$$H_{\rm cd}=-D_0\mathbf{N}^4+H_0\mathbf{N}^6, \tag{8}$$

$$H_{\rm LD}=\tfrac{1}{2}(p+2q)(e^{2i\phi}S_-J_-+e^{-2i\phi}S_+J_+) -\tfrac{1}{2}q(e^{2i\phi}J_-^2+e^{-2i\phi}J_+^2), \tag{9}$$

$$H_{\rm cdLD}=\tfrac{1}{4}(p_D+2q_D)[\mathbf{N}^2,e^{2i\phi}S_-J_-+e^{-2i\phi}S_+J_+]_+, \tag{10}$$

$$H_{\rm hfs}=aI_zL_z+b(I_xS_x+I_yS_y)+(b+c)I_zS_z +\tfrac{1}{2}d(e^{-2i\phi}I_+S_++e^{2i\phi}I_-S_-), \tag{11}$$

$$H_Z=g_L\mu_BB_0L_Z+g_S\mu_BB_0S_Z-g_r\mu_BB_0N_Z +g_l\mu_B(S_xB_x+S_yB_y)-g_N\mu_NB_0I_Z -g_r'\mu_B(e^{-2i\phi}N_+B_++e^{2i\phi}N_-B_-) +g_l'\mu_B(e^{-2i\phi}S_+B_++e^{2i\phi}S_-B_-). \tag{12}$$

$H_{\rm so}$ is the spin–orbit operator including the centrifugal distortion correction. $H_{\rm rot}$ is the rotational operator and $H_{\rm cd}$ is the rotational centrifugal distortion contribution. $H_{\rm LD}$ is the lambda-doubling term and $H_{\rm cdLD}$ its centrifugal distortion correction. $H_{\rm hfs}$ represents the magnetic hyperfine interaction Hamiltonian and H_Z is the Zeeman Hamiltonian.

The selection rules for LMR transitions are $\Delta J=0,\ \pm1$, $\Delta M_I=0$, $\Delta M_J=0,\ \pm1$. If the laser magnetic field (or electric field in case of electric dipole transitions) is parallel to the external magnetic field the selection rule $\Delta M_J=0$ applies. If they are perpendicular $\Delta M_J=\pm1$ holds. As pointed out by Brown, Carrington, and Sears,[5] the optimum polarization is parallel for Q transitions and perpendicular for R and P transitions. This rule has been experimentally confirmed by our spectra. Only for the $R(4\frac{1}{2})$, $Q(1\frac{1}{2})$, and $Q(2\frac{1}{2})$ transitions have equally intense lines been detected in both parallel and perpendicular polarizations.

The data have been analyzed using a linearized least-squares procedure. Since the Zeeman effect mixes energy levels with different J according to the selection rule $\Delta J=\pm1$, a suitably truncated basis set for the matrix of the Hamiltonian must be chosen ($\Delta J=\pm2$ in our case) in order to ensure that the calculations are accurate enough. H_0 was fixed to a calculated value (see Ref. 17) and p_D+2q_D was constrained to the previous value determined in Ref. 3. The observed lines are given in Table II. For each rotational transition, identified by the usual notation $P(J)$, $Q(J)$ or $R(J)$, the lower level is labeled by the quantum numbers M_J and M_I, and the upper level by F and M_F. The parity is defined for both levels, according to the selection rule for magnetic dipole transitions $\pm\leftarrow\pm$. For each transition the laser frequency, the differences observed–calculated from the fit, the tuning rates, and the weights are also given. The tuning rate, defined as the variation of the transition frequency with respect to the magnetic flux density B_0, is in MHz/mT. We chose to give a weight of 0.1 to the transitions with o–c between 6 and 10 MHz and a weight of 0 to the transitions with o–c greater than 10 MHz; virtually all these data points corresponded to resonances at high magnetic fields where the measurements are less accurate. The quality of the fit (Table III) is satisfactory and only a few lines, mostly partially overlapped or at high fields, have been given a lower weight. The standard deviation of the fit is 1.9 MHz, consistent with the expected experimental uncertainty.

We fitted A_D and constrained γ to zero, but in principle an equivalent fit can be made with the opposite choice. When we tried such a calculation, we obtained a significant worsening of the quality of the fit with a standard deviation of 3.0 MHz. Since we are confident that our set of data is not affected by severe systematic errors, this suggests that there are may be other contributions from parameters not accounted for in the effective Hamiltonian (see Discussion and Conclusions).

DISCUSSION AND CONCLUSIONS

The main goal of the present work was the determination of the spin–orbit coupling constant A_0 for FO in its ground $^2\Pi$ state. This parameter has been determined with great accuracy and the fit as a whole shows a marked improvement in the precision of most of the other parameters. The two exceptions are the rotational and centrifugal distortion con-

TABLE II. The $^2\Pi_{1/2} \leftarrow {}^2\Pi_{3/2}$ transitions of FO observed by far-infrared LMR.

	F	M_F	$\leftarrow$	M_I	M_J	p	ν_L (MHz)	B_0 (mT)	o−c (MHz)	$\partial\nu/\partial B_0$ (MHz/mT)	wt
$P(2\frac{1}{2})$	2	2		1/2	5/2	−	5 764 826.7	1778.74	−0.9	−10.9	1.0
	2	1		−1/2	5/2	−		1807.11	−0.0	−10.9	1.0
	1	1		−1/2	5/2	−		1831.51	−0.0	−10.9	1.0
	1	1		−1/2	5/2	+		1839.71	−8.7	−10.9	0.1
	2	2		1/2	5/2	+		1880.46	−0.6	−10.9	1.0
$P(1\frac{1}{2})$	0	0		−1/2	3/2	−	5 823 660.9	1489.17	−2.0	−15.1	1.0
	1	1		1/2	3/2	+		1501.60	−2.3	−15.0	1.0
	0	0		−1/2	3/2	+		1528.97	1.5	−15.0	1.0
	1	1		1/2	3/2	−		1545.84	−0.2	−15.0	1.1
	1	0		−1/2	3/2	−		1571.73	−0.3	−14.9	1.0
$Q(1\frac{1}{2})$	2	2		1/2	1/2	−	5 921 366.7	1295.46	3.7	−15.4	1.0
	2	1		−1/2	3/2	−		1321.56	−2.1	−15.4	1.0
	1	1		−1/2	3/2	−		1339.43	3.2	−15.4	1.0
	1	1		−1/2	3/2	+		1346.74	−0.1	−15.4	1.0
	2	2		1/2	3/2	+		1369.56	−0.9	−15.4	1.0
	2	1		−1/2	3/2	+		1400.17	2.2	−15.3	1.0
	2	1		1/2	3/2	−		1301.42	3.6	−15.4	1.0
	1	1		1/2	3/2	−		1318.74	−0.6	−15.4	1.0
	1	1		1/2	3/2	+		1326.25	−2.4	−15.4	1.0
	2	0		−1/2	3/2	−		1328.14	−2.1	−15.3	1.0
	1	0		−1/2	3/2	−		1348.31	3.6	−15.3	1.0
	1	0		−1/2	3/2	+		1360.90	−0.5	−15.3	1.0
	2	1		1/2	3/2	+		1379.70	−1.1	−15.3	1.0
	2	0		−1/2	3/2	+		1408.18	−41.9	−15.2	0.0
$Q(2\frac{1}{2})$	3	3		1/2	5/2	+	5 921 366.7	1908.66	−1.6	−10.9	1.0
	3	2		−1/2	5/2	+		1940.85	−0.2	−10.9	1.0
	2	2		−1/2	5/2	+		1968.26	7.6	−10.9	0.1
	2	2		−1/2	5/2	−		2017.10	9.8	−10.9	0.1
	3	3		1/2	5/2	−		2051.37	18.9	−10.9	0.0
	3	2		−1/2	5/2	−		2091.93	30.5	−10.8	0.0
	3	2		1/2	5/2	+		1924.56	1.7	−10.9	1.0
	2	2		1/2	5/2	+		1951.24	−0.0	−10.9	1.0
	3	1		−1/2	5/2	+		1958.09	−0.2	−10.8	1.0
	2	1		−1/2	5/2	+		1990.43	8.0	−10.7	0.1
	2	1		−1/2	5/2	−		2046.38	17.3	−10.8	0.0
	3	2		1/2	5/2	−		2075.70	25.6	−10.8	0.0
$Q(11\frac{1}{2})$	12	−12		−1/2	−23/2	+	5 999 028.8	1202.87	1.8	7.0	1.0
	11	−11		1/2	−23/2	+		1259.35	−0.4	7.0	1.0
	12	−11		−1/2	−21/2	+		1315.06	−0.3	6.4	1.0
	11	−10		1/2	−21/2	+		1379.02	10.2	6.4	1.0
	12	−10		−1/2	−19/2	+		1449.60	1.3	5.8	1.0
	12	−9		1/2	−19/2	+		1460.84	−4.8	5.7	1.0
	11	−9		1/2	−19/2	+		1527.57	−0.4	5.8	1.0
	12	−9		−1/2	−17/2	+		1615.16	1.1	5.2	1.0
	12	−8		−1/2	−15/2	+		1819.88	16.4	4.6	0.0
$Q(12\frac{1}{2})$	12	−12		1/2	−25/2	−	5 999 028.8	76.05	0.3	6.8	1.0
	12	−11		1/2	−23/2	−		82.72	1.4	6.2	1.0
	12	−10		1/2	−21/2	−		91.19	−0.2	5.7	1.0
	12	−9		1/2	−19/2	−		101.14	0.0	5.1	1.0
	12	−8		1/2	−17/2	−		113.47	0.5	4.6	1.0
	12	−7		1/2	−15/2	−		129.21	1.8	4.0	1.0
	12	−6		1/2	−13/2	−		151.01	−1.8	3.5	1.0
	12	−5		1/2	−11/2	−		179.55	−0.2	2.9	1.0
	12	−4		1/2	−9/2	−		221.75	0.6	2.4	1.0
	12	−12		1/2	−25/2	+		801.68	3.9	6.9	1.0
	12	−11		1/2	−23/2	+		872.30	2.4	6.3	1.0
	13	−13		−1/2	−25/2	+		886.49	2.5	6.9	1.0
	12	−10		1/2	−21/2	+		956.49	0.3	5.8	1.0
	13	−12		−1/2	−23/2	+		962.55	−0.2	6.3	1.0
	13	−11		−1/2	−21/2	+		1052.16	1.1	5.8	1.0
	12	−9		1/2	−19/2	+		1057.70	1.8	5.2	1.0
	13	−10		−1/2	−19/2	+		1160.24	2.5	5.3	1.0

TABLE II. (*Continued*.)

	F	M_F	←	M_I	M_J	p	ν_L (MHz)	B_0 (mT)	o−c (MHz)	$\partial\nu/\partial B_0$ (MHz/mT)	wt
	12	−8		1/2	−17/2	+		1182.77	2.6	4.7	1.0
	13	−9		−1/2	−17/2	+		1294.27	−1.2	4.7	1.0
	12	−7		1/2	−15/2	+		1341.81	0.0	4.1	1.0
	13	−8		−1/2	−15/2	+		1460.84	4.5	4.2	1.0
$Q(13\frac{1}{2})$	14	14		1/2	27/2	−	5 999 028.8	344.58	−0.8	−6.7	1.0
	14	13		−1/2	27/2	−		363.21	−0.2	−6.6	1.0
	14	13		1/2	25/2	−		373.29	−1.5	−6.3	1.0
	14	12		−1/2	25/2	−		391.33	−1.7	−6.1	1.0
	14	12		1/2	23/2	−		406.33	−2.8	−5.8	1.0
	14	11		−1/2	23/2	−		425.02	−1.1	−5.6	1.0
	13	13		−1/2	27/2	−		430.28	−2.5	−6.7	1.0
	13	13		1/2	25/2	−		445.45	5.8	−6.4	1.0
	14	11		1/2	21/2	−		445.45	−3.7	−5.3	1.0
	13	12		−1/2	25/2	−		464.82	1.1	−6.2	1.0
	14	10		−1/2	21/2	−		464.82	−3.2	−5.1	1.0
	13	12		1/2	23/2	−		483.47	−2.8	−5.9	1.0
	14	10		1/2	19/2	−		493.09	−2.4	−4.8	1.0
	13	11		−1/2	23/2	−		504.70	−0.5	−5.7	1.0
	14	9		−1/2	19/2	−		514.34	−0.2	−4.6	1.0
	13	11		1/2	21/2	−		530.20	−2.5	−5.4	1.0
	14	9		1/2	17/2	−		552.67	2.8	−4.3	1.0
	13	10		−1/2	21/2	−		552.67	−0.9	−5.2	1.0
	14	8		−1/2	17/2	−		575.27	0.6	−4.1	1.0
	13	10		1/2	19/2	−		586.77	−1.5	−4.8	1.0
	13	9		−1/2	19/2	−		610.99	−1.6	−4.7	1.0
	13	13		−1/2	27/2	+		1217.35	1.1	−6.7	1.0
	14	14		1/2	27/2	+		1275.29	−1.6	−6.7	1.0
	13	12		−1/2	25/2	+		1315.06	−2.1	−6.2	1.0
	14	13		1/2	25/2	+		1378.55	−0.2	−6.2	1.0
	13	11		−1/2	23/2	+		1431.23	0.7	−5.6	1.0
	14	12		1/2	23/2	+		1499.58	−0.6	−5.7	1.0
	13	10		−1/2	21/2	+		1569.16	−1.4	−5.1	1.0
	14	11		1/2	21/2	+		1643.86	−1.4	−5.2	1.0
	13	9		−1/2	19/2	+		1737.59	−0.8	−4.6	1.0
$Q(14\frac{1}{2})$	15	15		1/2	29/2	+	5 999 028.8	1674.97	−0.1	−6.7	1.0
	15	14		−1/2	29/2	+		1709.27	−23.2	−6.5	0.0
	14	14		−1/2	29/2	+		1763.83	0.3	−6.6	1.0
	15	14		1/2	27/2	+		1799.81	−0.1	−6.2	1.0
$Q(15\frac{1}{2})$	16	−16		−1/2	−31/2	+	6 032 811.3	810.90	2.9	7.2	1.0
	15	−15		1/2	−31/2	+		863.66	3.1	7.2	1.0
	16	−14		1/2	−29/2	+		865.51	−1.8	6.6	1.0
	15	−14		1/2	−29/2	+		924.37	−0.7	6.8	1.0
	16	−14		−1/2	−27/2	+		928.42	1.1	6.3	1.0
	15	−13		1/2	−27/2	+		993.28	0.6	6.3	1.0
	16	−13		−1/2	−25/2	+		1000.87	0.5	5.9	1.0
	15	−12		1/2	−25/2	+		1073.72	−1.0	5.8	1.0
	16	−12		−1/2	−23/2	+		1085.70	−1.0	5.4	1.0
	15	−11		1/2	−23/2	+		1167.48	1.1	5.4	1.0
	16	−11		−1/2	−21/2	+		1185.35	1.4	5.0	1.0
	15	−15		1/2	−31/2	−		1718.98	−3.2	7.3	1.0
	16	−16		−1/2	−31/2	−		1798.69	−1.4	7.3	1.0
	15	−14		1/2	−29/2	−		1836.54	−0.1	6.8	1.0
	16	−15		−1/2	−29/2	−		1920.37	−4.3	6.9	1.0
	15	−13		1/2	−27/2	−		1972.59	−5.7	6.4	1.0
	16	−14		−1/2	−27/2	−		2060.53	−13.8	6.4	0.0
$Q(16\frac{1}{2})$	16	16		−1/2	33/2	−	6 032 811.3	609.55	−0.8	−7.1	1.0
	16	16		1/2	31/2	−		626.29	0.3	−6.9	1.0
	16	15		−1/2	31/2	−		648.58	−1.5	−6.7	1.0
	17	17		1/2	33/2	−		662.77	−2.5	−7.1	1.0
	16	15		1/2	29/2	−		669.42	−3.4	−6.4	1.0
	16	14		−1/2	29/2	−		693.86	2.0	−6.3	1.0
	17	16		1/2	31/2	−		706.80	1.5	−6.7	1.0
	16	13		−1/2	27/2	−		745.23	0.9	−5.8	1.0

TABLE II. (*Continued*.)

	F	M_F	←	M_I	M_J	p	ν_L (MHz)	B_0 (mT)	o−c (MHz)	$\partial\nu/\partial B_0$ (MHz/mT)	wt
	17	15		1/2	29/2	−		756.03	0.5	−6.3	1.0
	16	12		−1/2	25/2	−		805.15	0.4	−5.4	1.0
	16	11		−1/2	23/2	−		876.15	1.8	−4.9	1.0
	17	13		1/2	25/2	−		878.95	3.7	−5.4	1.0
	17	12		1/2	23/2	−		955.30	−0.5	−5.0	1.0
	16	10		−1/2	21/2	−		960.10	−1.1	−4.5	1.0
	17	11		1/2	21/2	−		1047.05	−1.2	−4.5	1.0
	16	9		−1/2	19/2	−		1062.83	−1.8	−4.0	1.0
	17	10		1/2	19/2	−		1158.74	−0.2	−4.1	1.0
	16	−16		1/2	−33/2	+		293.31	−0.5	7.2	1.0
	16	−15		1/2	−31/2	+		312.55	−0.5	6.8	1.0
	16	−14		1/2	−29/2	+		334.15	1.5	6.3	1.0
	16	−13		1/2	−27/2	+		359.29	1.7	5.9	1.0
	17	−17		−1/2	−33/2	+		374.34	1.4	7.2	1.0
	16	−12		1/2	−25/2	+		388.48	2.0	5.4	1.0
	17	−16		−1/2	−31/2	+		397.93	2.0	6.8	1.0
	17	−15		−1/2	−29/2	+		424.52	3.8	6.4	1.0
	17	−14		−1/2	−27/2	+		455.51	2.5	5.9	1.0
	16	−10		1/2	−11/2	+		463.75	2.3	4.6	1.0
	17	−13		−1/2	−25/2	+		491.54	0.2	5.5	1.0
	16	−9		1/2	−19/2	+		513.53	1.7	4.1	1.0
	17	−12		−1/2	−23/2	+		533.08	1.0	5.1	1.0
	16	−8		1/2	−17/2	+		575.01	1.4	3.7	1.0
	17	−11		−1/2	−21/2	+		582.56	0.9	4.6	1.0
	17	−10		−1/2	−19/2	+		641.78	2.6	4.2	1.0
$Q(17\frac{1}{2})$	18	18		1/2	35/2	−	6 032 811.3	1122.30	1.9	−7.1	1.0
	18	17		1/2	33/2	−		1190.75	1.4	−6.7	1.0
	17	17		−1/2	35/2	−		1204.42	0.0	−7.1	1.0
	18	16		1/2	31/2	−		1267.72	−1.3	−6.3	1.0
	17	16		−1/2	33/2	−		1278.89	2.7	−6.7	1.0
	18	15		1/2	29/2	−		1356.06	0.3	−5.9	1.0
	17	15		−1/2	31/2	−		1362.49	0.5	−6.3	1.0
	18	−18		−1/2	−35/2	+	6 061 914.8	1752.14	−0.5	7.7	1.0
	17	−17		1/2	−35/2	+		1801.61	−0.6	7.7	1.0
	18	−17		−1/2	−33/2	+		1855.28	−1.7	7.2	1.0
	17	−16		1/2	−33/2	+		1911.05	−1.6	7.2	1.0
	18	−16		−1/2	−33/2	+		1971.43	−4.4	6.8	1.0
$Q(18\frac{1}{2})$	19	−19		−1/2	−39/2	−	6 061 914.8	187.80	−0.9	7.6	1.0
	19	−18		−1/2	−35/2	−		198.06	0.7	7.2	1.0
	19	−17		−1/2	−33/2	−		209.73	1.1	6.8	1.0
	19	−16		−1/2	−31/2	−		222.81	1.9	6.4	1.0
	18	−18		1/2	−39/2	−		236.68	−0.9	7.6	1.0
	19	−15		−1/2	−29/2	−		236.68	8.5	6.0	0.1
	18	−17		1/2	−35/2	−		250.22	0.8	7.2	1.0
	19	−14		−1/2	−27/2	−		255.23	0.2	5.6	1.0
	18	−16		1/2	−33/2	−		265.56	1.5	6.7	1.0
	19	−13		−1/2	−25/2	−		275.34	−1.2	5.2	1.0
	18	−15		1/2	−31/2	−		283.25	0.1	6.3	1.0
	19	−12		−1/2	−23/2	−		298.39	−0.4	4.8	1.0
	18	−14		1/2	−29/2	−		303.08	0.6	5.9	1.0
	18	−13		1/2	−27/2	−		325.72	2.1	5.5	1.0
	18	−12		1/2	−25/2	−		352.30	2.2	5.1	1.0
	18	−18		1/2	−37/2	+		1193.59	0.1	7.7	1.0
	18	−17		1/2	−35/2	+		1261.52	1.7	7.2	1.0
	19	−19		−1/2	−39/2	+		1270.12	2.1	7.7	1.0
	18	−16		1/2	−33/2	+		1338.14	−0.3	6.8	1.0
	19	−18		−1/2	−37/2	+		1341.41	0.8	7.3	1.0
	19	−17		−1/2	−33/2	+		1421.10	−0.1	6.9	1.0
	18	−15		1/2	−31/2	+		1424.26	−0.6	6.4	1.0
	19	−16		−1/2	−33/2	+		1511.31	−4.4	6.5	1.0
	18	−14		1/2	−29/2	+		1521.91	0.1	6.0	1.0
	19	−15		−1/2	−29/2	+		1612.11	0.4	6.1	1.0
	18	−13		1/2	−27/2	+		1634.15	−1.4	5.6	1.0
	19	−14		−1/2	−27/2	+		1728.14	0.9	5.7	1.0

TABLE II. (*Continued*.)

	F	M_F	←	M_I	M_J	p	ν_L (MHz)	B_0 (mT)	o−c (MHz)	$\partial\nu/\partial B_0$ (MHz/mT)	wt
	18	−12		1/2	−25/2	+		1763.25	0.7	5.2	1.0
	19	−13		−1/2	−25/2	+		1862.28	0.2	5.3	1.0
	18	−11		1/2	−23/2	+		1914.85	−0.2	4.8	1.0
$Q(19\frac{1}{2})$	20	20		1/2	39/2	−	6 061 914.8	309.61	−3.0	−7.6	1.0
	20	19		−1/2	39/2	−		325.72	−18.0	−7.3	0.0
	20	19		1/2	37/2	−		328.28	30.7	−7.4	0.0
	20	18		−1/2	37/2	−		341.22	0.1	−7.0	1.0
	20	18		1/2	35/2	−		347.45	−0.2	−6.9	1.0
	20	17		−1/2	35/2	−		360.55	0.8	−6.6	1.0
	20	17		1/2	33/2	−		368.91	−0.1	−6.5	1.0
	20	16		−1/2	33/2	−		382.74	4.0	−6.3	1.0
	19	19		−1/2	39/2	−		386.61	−2.5	−7.6	1.0
	20	16		1/2	31/2	−		392.31	−4.4	−6.1	1.0
	19	19		1/2	37/2	−		392.31	−0.8	−7.4	1.0
	20	15		−1/2	31/2	−		407.15	2.8	−5.9	1.0
	19	18		−1/2	37/2	−		407.15	−2.3	−7.2	1.0
	19	18		1/2	35/2	−		414.90	−3.5	−7.0	1.0
	20	15		1/2	29/2	−		420.80	2.3	−5.7	1.0
	19	17		−1/2	35/2	−		430.09	−3.0	−6.8	1.0
	20	14		−1/2	29/2	−		434.72	−0.1	−5.5	1.0
	19	19		−1/2	39/2	+		1384.91	0.2	−7.5	1.0
	20	20		1/2	39/2	+		1434.02	−1.2	−7.5	1.0
	19	18		−1/2	37/2	+		1460.83	0.9	−7.1	1.0
	20	19		1/2	37/2	+		1512.73	−0.0	−7.1	1.0
	19	17		−1/2	35/2	+		1545.44	0.1	−6.7	1.0
	19	16		−1/2	33/2	+		1640.69	−0.3	−6.3	1.0
	20	17		1/2	33/2	+		1698.87	−0.1	−6.3	1.0
	19	15		−1/2	31/2	+		1748.60	−0.9	−5.9	1.0
	20	16		1/2	31/2	+		1810.30	−0.2	−5.9	1.0
	19	14		−1/2	29/2	+		1872.13	−0.4	−5.5	1.0
	20	15		1/2	29/2	+		1937.50	−0.4	−5.5	1.0
$Q(20\frac{1}{2})$	21	21		1/2	41/2	+	6 061 914.8	1941.29	−0.8	−7.5	1.0
$R(2\frac{1}{2})$	4	4		1/2	5/2	−	6 153 279.0	992.23	−0.1	−11.9	1.0
	4	3		−1/2	5/2	−		1021.04	−1.3	−11.8	1.0
	3	3		−1/2	5/2	−		1049.00	−3.7	−11.9	1.0
	3	3		−1/2	5/2	+		1137.92	−7.5	−11.9	0.1
	4	4		1/2	5/2	+		1164.58	−5.3	−11.9	1.0
	4	3		1/2	3/2	−		1619.03	3.5	−7.6	1.0
	4	2		−1/2	3/2	−		1656.23	0.6	−7.5	1.0
	3	3		1/2	3/2	−		1659.37	0.2	−7.6	1.0
	3	2		−1/2	3/2	−		1702.18	−1.1	−7.5	1.0
	3	2		−1/2	3/2	+		1838.23	−7.7	−7.6	0.1
	4	3		1/2	3/2	+		1886.63	−8.0	−7.6	0.1
$R(4\frac{1}{2})$	6	5		1/2	9/2	−	6 290 222.3	779.39	−1.1	−8.6	1.0
	6	4		−1/2	9/2	−		808.68	−3.2	−8.4	1.0
	5	4		−1/2	9/2	−		854.26	−1.5	−8.5	1.0
	6	4		1/2	7/2	−		1000.02	−0.6	−6.7	1.0
	6	3		−1/2	7/2	−		1033.72	−2.7	−6.6	1.0
	5	4		1/2	7/2	−		1055.61	−1.2	−6.8	1.0
	5	4		−1/2	9/2	+		1085.58	−1.2	−8.5	1.0
	5	3		−1/2	7/2	−		1092.89	−1.8	−6.6	1.0
	6	5		1/2	9/2	+		1126.59	1.6	−8.5	1.0
	5	3		−1/2	7/2	+		1387.42	−1.0	−6.6	1.0
	6	3		1/2	5/2	−		1387.42	0.0	−4.9	1.0
	6	4		1/2	7/2	+		1441.53	0.2	−6.7	1.0
	6	2		−1/2	5/2	−		1432.74	−0.6	−4.8	1.0
	5	3		1/2	5/2	−		1465.07	−1.3	−4.9	1.0
	6	3		−1/2	7/2	+		1485.11	−0.2	−6.5	1.0
	5	2		−1/2	5/2	−		1517.31	−0.0	−4.8	1.0
	5	2		−1/2	5/2	+		1918.91	−0.5	−4.9	1.0
	6	3		1/2	5/2	+		1991.95	2.8	−4.9	1.0
	6	6		1/2	9/2	−		768.28	−1.2	−8.7	1.0

TABLE II. (*Continued.*)

	F	M_F	←	M_I	M_J	p	ν_L (MHz)	B_0 (mT)	o–c (MHz)	$\partial\nu/\partial B_0$ (MHz/mT)	wt
	6	5		−1/2	9/2	−		797.13	−1.9	−8.5	1.0
	5	5		−1/2	9/2	−		840.46	0.2	−8.6	1.0
	6	5		1/2	7/2	−		981.96	−0.8	−6.8	1.0
	6	4		−1/2	7/2	−		1015.14	0.3	−6.7	1.0
	5	5		1/2	7/2	−		1034.24	0.1	−6.9	1.0
	5	5		−1/2	9/2	+		1066.23	0.5	−8.6	1.0
	5	4		−1/2	7/2	−		1070.53	0.9	−6.8	1.0
	6	6		1/2	9/2	+		1108.19	−0.7	−8.6	1.0
	6	5		−1/2	9/2	+		1142.79	1.2	−8.5	1.0
	5	5		1/2	7/2	+		1313.29	0.4	−7.0	1.0
	5	4		−1/2	7/2	+		1356.19	1.7	−6.8	1.0
	6	4		1/2	5/2	−		1354.08	3.1	−5.0	1.0
	6	3		−1/2	5/2	−		1396.86	0.3	−4.9	1.0
	6	5		1/2	7/2	+		1411.98	−0.0	−6.8	1.0
	5	4		1/2	5/2	−		1424.55	−0.9	−5.1	1.0
	6	4		−1/2	7/2	+		1454.28	1.7	−6.7	1.0
	5	3		−1/2	5/2	−		1473.89	−1.2	−4.9	1.0
	5	4		1/2	5/2	+		1798.48	−1.2	−5.2	1.0
	5	3		−1/2	5/2	+		1859.66	−0.9	−5.0	1.0
	6	4		1/2	5/2	+		1936.67	2.1	−5.1	1.0
	6	3		−1/2	5/2	+		1997.68	6.9	−4.9	0.1
$R(7\frac{1}{2})$	9	9		1/2	15/2	+	6 493 911.5	695.29	−0.3	−7.0	1.0
	8	8		−1/2	15/2	+		780.13	0.4	−7.0	1.0
	9	8		1/2	13/2	+		800.33	−1.7	−6.1	1.0
	8	7		−1/2	13/2	+		896.64	0.5	−6.1	1.0
	9	7		1/2	11/2	+		942.44	0.3	−5.2	1.0
	9	6		−1/2	11/2	+		976.75	−0.7	−5.1	1.0
	8	6		−1/2	11/2	+		1054.80	0.3	−5.2	1.0
	9	6		1/2	9/2	+		1143.76	−0.2	−4.3	1.0
	9	5		−1/2	9/2	+		1186.25	1.4	−4.2	1.0
	8	6		1/2	9/2	+		1234.53	1.3	−4.4	1.0
	8	8		−1/2	15/2	−		1242.78	1.4	−7.0	1.0
	8	5		−1/2	9/2	+		1282.22	2.1	−4.2	1.0
	9	9		1/2	15/2	−		1298.19	1.7	−7.0	1.0
	8	7		−1/2	13/2	−		1428.20	0.7	−6.1	1.0
	9	8		1/2	13/2	−		1492.57	1.3	−6.1	1.0
	9	4		−1/2	7/2	+		1509.75	0.6	−3.3	1.0
	8	6		−1/2	11/2	−		1679.09	−0.1	−5.2	1.0
	9	7		1/2	11/2	−		1754.51	0.5	−5.2	1.0

stants B_0 and D_0, which are better determined in the Fourier transform investigation,[4] possibly because more high-J lines were included. The determination of the full set of magnetic hyperfine parameters arises from the detection of resolved hyperfine structures involving both spin states and both lambda doublets. All these parameters have been fitted in the present analysis and are shown in Table III. The zero-field transitions predicted using the final parameters of Table III are given in Table IV.

The magnitude $|A|$ of the spin–orbit interaction term can be estimated from the atomic spin–orbit constants ξ_F and ξ_O according to the equation

$$|A| = c_F^2|\xi_F| + c_O^2|\xi_O|, \tag{13}$$

once the expansion coefficients of the atomic orbitals are known. Where possible, the coefficient c_F is evaluated from the hyperfine structure parameters. Although several methods have been used in previous work,[18,19] we think that the most reliable procedure is based on the relationship $c_F^2 = \frac{2}{3}h_{3/2}/A_{3/2}$, where $A_{3/2}$ is the magnetic hyperfine parameter determinable for atomic F in the $^2P_{3/2}$ state and $h_{3/2}$ is equal to $a+(1/2)(b+c)$. If the overlap integral is included,[18] c_F^2 and c_O^2 turn out to be 0.226 and 0.844, respectively, and $|A|$ is 188 cm^{-1}, which is close to the experimental value. If the calculation is repeated with different methods (such as estimating c_F from atomic and molecular values for the $J=\frac{1}{2}$ and $\Omega=\frac{1}{2}$ components), $|A|$ varies between 176 and 206 cm^{-1}.

The lambda-doubling parameters have been reliably determined; however, the set of data is not extended enough to allow the determination of the centrifugal distortion correction, which has been constrained to the literature value.[3]

The magnetic hyperfine constants are related to the electronic wave functions[20] and provide useful information on the distribution of the unpaired electron(s) in the molecule. The hyperfine parameter a is related to the orbital distribution $\langle r^{-3}\rangle_l$, where r is the distance between the unpaired electron and the F nucleus; the Fermi contact parameter b_F is a measure of the spin density at the nucleus $|\Psi(0)|^2$; c and d are associated to the angular spin distribution, $\langle(3\cos^2\theta$

TABLE III. Molecular parameters obtained for FO in the $^2\Pi$ state.

Parameter[a]	This work	Previous works
B_0	31 539.819(94)	31 539.450(33)[b]
D_0	0.129 79(44)	0.128 935(33)[b]
$10^7 H_0$	−0.39[e]	
A_0/cm^{-1}	−196.108 686(50)	−193.28(97)[b]
A_D	12.052(10)	16.8(16)[b]
$p+2q$	428.104(61)	438.7(18)[b]
$10^2(p_D+2q_D)$	−0.45	−0.45(120)[c]
q	−1.5255(94)	−2.1[b]
a	779.4(16)	696(18)[d]
b	406.3(20)	
$b+c$	−196.1(22)	
d	977.79(46)	
g_L	0.999 34(14)	
g_S	2.001 11(22)	
$10^1 g_l$	0.112 7(28)	
$10^4 g_r$	−0.93(17)	
$10^4 g_r'$	0.477(68)	
$10^2(g_l'-g_r')$	0.688 6(37)	
g_N	5.257 73	
σ[f]	1.9	
No. of trans.	290	

[a]Values in MHz where appropriate. The numbers in parentheses represent one standard deviation of the least-squares fit, in units of the last quoted decimal place. Parameters with no standard deviation are held fixed in the present analysis.
[b]Reference 4.
[c]Reference 3.
[d]Reference 1. This is a value for $h_{3/2}=a+1/2(b+c)$. Our value for this parameter is 681.4(19) MHz.
[e]Calculated value.
[f]σ is the overall standard deviation of the fit.

TABLE IV. Predicted fine-structure transitions of FO in zero magnetic field.

Transition	ν (MHz)	p	ν (MHz)	p
$P(10\frac{1}{2})$	5 317 782.5	+	5 313 496.8	−
$P(9\frac{1}{2})$	5 370 246.3	+	5 374 103.4	−
$P(8\frac{1}{2})$	5 431 083.1	+	5 427 654.6	−
$P(7\frac{1}{2})$	5 485 721.6	+	5 488 721.5	−
$P(6\frac{1}{2})$	5 547 018.2	+	5 544 447.0	−
$P(5\frac{1}{2})$	5 603 829.9	+	5 605 972.3	−
$P(4\frac{1}{2})$	5 665 583.0	+	5 663 869.2	−
$P(3\frac{1}{2})$	5 724 563.5	+	5 725 848.7	−
$P(2\frac{1}{2})$	5 786 767.6	+	5 785 911.0	−
$P(1\frac{1}{2})$	5 847 909.6	+	5 848 337.9	−
$Q(1\frac{1}{2})$	5 943 652.0	+	5 942 796.2	−
$Q(2\frac{1}{2})$	5 944 193.1	+	5 945 475.9	−
$Q(3\frac{1}{2})$	5 947 942.2	+	5 946 233.5	−
$Q(4\frac{1}{2})$	5 948 916.4	+	5 951 049.5	−
$Q(5\frac{1}{2})$	5 954 796.2	+	5 952 240.4	−
$Q(6\frac{1}{2})$	5 956 203.9	+	5 959 180.1	−
$Q(7\frac{1}{2})$	5 964 198.9	+	5 960 804.8	−
$Q(8\frac{1}{2})$	5 966 040.8	+	5 969 850.0	−
$Q(9\frac{1}{2})$	5 976 130.2	+	5 971 909.3	−
$Q(10\frac{1}{2})$	5 978 407.1	+	5 983 036.3	−
$R(1\frac{1}{2})$	6 101 077.5	+	6 102 361.2	−
$R(2\frac{1}{2})$	6 167 571.8	+	6 165 860.7	−
$R(3\frac{1}{2})$	6 231 275.6	+	6 233 413.8	−
$R(4\frac{1}{2})$	6 299 882.6	+	6 297 317.5	−
$R(5\frac{1}{2})$	6 363 981.8	+	6 366 973.5	−
$R(6\frac{1}{2})$	6 434 681.1	+	6 431 263.4	−
$R(7\frac{1}{2})$	6 499 156.6	+	6 503 000.2	−
$R(8\frac{1}{2})$	6 571 924.8	+	6 567 655.8	−
$R(9\frac{1}{2})$	6 636 754.9	+	6 641 448.8	−
$R(10\frac{1}{2})$	6 711 565.7	+	6 706 447.3	−

$-1)/r^3\rangle_s$ and $\langle(\sin^2\theta)/r^3\rangle_s$, respectively, where θ is the angle between the vector **r** and the internuclear axis. The above-mentioned expectation values for FO, CF,[21] and the F atom[22] are given in Table V.

The spin average $\langle r^{-3}\rangle_s$ can be calculated from $d+c/3$ by giving $\langle\pi|\sin^2\theta|\pi\rangle$ a value of 4/5 and $\langle\pi|3\cos^2\theta-1|\pi\rangle$ a value of $-2/5$, which are correct for atomic p_π orbitals and good approximations for molecular π orbitals. The ratios $\langle r^{-3}\rangle_s:\langle(3\cos^2\theta-1)/r^3\rangle_s:\langle(\sin^2\theta)/r^3\rangle_s$, expected to be 1: −0.4: 0.8 for a p_π atomic orbital are 1: −0.52: 0.84 for FO and 1: −0.35: 0.78 for CF.[14] These values, greater than the corresponding atomic ratios, suggest that the unpaired electron in FO is in an orbital which is slightly polarized from a pure p orbital.

A full set of g factors, shown in Table III, has been determined in the present work (see Refs. 16 and 23 for a detailed description of the Zeeman parameters). Estimates of some of the g factors can be obtained from the relationships

$$g_l = -\gamma/2B, \tag{14}$$

$$g_l' \simeq p/2B, \tag{15}$$

$$g_r' \simeq -q/B, \tag{16}$$

$$g_l' - g_r' \simeq (p+2q)/2B. \tag{17}$$

The calculated values for g_r' (0.484×10^{-4}) and $g_l'-g_r'$ (0.6787×10^{-2}) are in excellent agreement with the observed values 0.477×10^{-4} and 0.6886×10^{-2}.

The orbital g factor g_L can be expressed as a sum of a main term (1.0) plus relativistic ($\langle\delta g_{\mathrm{rel}}\rangle_{\mathrm{av}}$), orbit–orbit ($\langle\delta g_{\mathrm{orb}}\rangle_{\mathrm{av}}$), and nonadiabatic ($\Delta g_L$) contributions.[10,24] The electron spin g factor corrected for quantum electrodynamic and relativistic effects is $g_S=2.002\,32(1+\langle\delta g_{\mathrm{rel}}\rangle_{\mathrm{av}})$. The relativistic correction can therefore be estimated from the experimental value for g_S and is -6.0×10^{-4} for FO. Assuming that the orbit–orbit and nonadiabatic contributions are negligible compared with the relativistic term,[10] g_L can be calculated using the relationship $g_L=1.0+\langle\delta g_{\mathrm{rel}}\rangle_{\mathrm{av}}=1.0-6.0\times10^{-4}=0.9994$, which is in excellent agreement with the experimental value 0.999 34(14). The nonadiabatic contribution can also be estimated from the relationship $\Delta g_L=q/2B$. The calculated value of 2.4×10^{-5} confirms that the contribution $\langle\delta g_{\mathrm{rel}}\rangle_{\mathrm{av}}$ is dominant. This relativistic contribution can be calculated from the corresponding

TABLE V. Hyperfine structure parameters (in MHz) and expectation values of distribution functions over the electronic wave function (in m^{-3}) of ^{19}F for FO, CF, and atomic fluorine.

Parameter	FO[a]	CF[b]	F[c]
a	779.4(16)	705.94(14)	
b_F	205.5(15)[d]	151.19(49)	
c	−602.4(30)[d]	−351.6(14)	
d	977.79(46)	792.195(98)	
$10^{-30}\langle r^{-3}\rangle_l$	10.485	9.502	4.96
$10^{-29}\Psi(0)^2$	3.2997	2.429	4.84
$10^{-30}\langle(3\cos^2\theta-1)/r^3\rangle_s$	−5.4027	−3.151	
$10^{-30}\langle(\sin^2\theta)/r^3\rangle_s$	8.7691	7.100	
$10^{-30}\langle r^{-3}\rangle_s$	10.452	9.075	5.49

[a]This work.
[b]Reference 21.
[c]Reference 22.
[d]Derived parameter.

atomic values for F[10] and O,[24] which are, respectively, -1.8 and -1.3×10^{-4}. It is given by

$$\langle \delta g_{\rm rel}\rangle_{\rm av,FO}=c_{\rm F}^2\langle \delta g_{\rm rel}\rangle_{\rm av,F}+c_{\rm O}^2\langle \delta g_{\rm rel}\rangle_{\rm av,O}, \tag{18}$$

using values for the coefficients $c_{\rm F}^2$ and $c_{\rm O}^2$ determined from the magnetic hyperfine parameters. The result is -1.5×10^{-4}, which is remarkably different from the experimental value of -6.0×10^{-4} but consistent with the values calculated by Veseth[25] for other molecules, such as OH, SH, NO, NS, and ClO.

If values for B and γ are known, the parameter g_l should be predictable from Curl's relationship, Eq. (14). Although we know the value for B very precisely, we have not determined a value for the spin–rotation parameter γ in our fit because it is completely correlated with the parameter A_D. Brown and Watson[26] have shown that, in a fit of the parameters of a $^2\Pi$ Hamiltonian to a set of data, one can either chose to constrain γ to zero and determine a value for the effective centrifugal distortion correction to the spin–orbit coupling $\tilde{A}_D$, where

$$\tilde{A}_D=A_D-\gamma\frac{2B}{(A-2B)} \tag{19}$$

or one can constrain A_D to zero and determine a value for an effective spin–rotation parameter $\tilde{\gamma}$, where

$$\tilde{\gamma}=\gamma-A_D\frac{(A-2B)}{2B}. \tag{20}$$

We can estimate the value for γ by using Eq. (20) and substituting the values of A_D (strictly $\tilde{A}_D$), A and B from Table III. This is actually a value for $\tilde{\gamma}$ but, if A_D happened to be very small, it would be close to the true value for γ. Substitution of this value in Eq. (14) gives a value for g_l of -0.018, which is very different from the experimental value of 0.011 27. Similar behavior is shown for the energy levels of CF;[21] the authors in that case suggested that the discrepancy was attributable to an inexact interpretation of the effective parameters in the Hamiltonian (in other words, the assumption which we have made that A_D is very small is not valid).

The constraint of the parameter A_D or γ to zero in the fit has the effect of modifying several parameters in the Hamiltonian. If we apply Brown and Watson's unitary transformation to the Zeeman Hamiltonian, we can show that the parameter g_l is one which is affected and so becomes an effective parameter $\tilde{g}_l$ where

$$\tilde{g}_l=g_l-\frac{\gamma}{(A-2B)}(g_L+g_S), \tag{21}$$

if γ is constrained to zero or

$$\tilde{g}_l=g_l-\frac{A_D}{2B}(g_L+g_S), \tag{22}$$

if A_D is constrained to zero. Thus the value determined in the fit, $\tilde{g}_l$, will differ from the value g_l according to whichever of these two two equations applies. If we accept the correctness of Curl's relationship, Eq. (14), and substitute for g_l in Eq. (21), we can rearrange the result to give an expression for γ in terms of experimentally determinable parameters:

$$\gamma=-\frac{2B(A-2B)\tilde{g}_l}{\{A-2B[1-(g_L+g_S)]\}}. \tag{23}$$

Substitution of values from Table III in Eq. (23) gives a value for γ (the true spin–rotation constant) of -734.3 MHz, from which we determine that the true value for $g_l=-\gamma/2B$ is 0.011 64. This latter value is now much closer to the effective value for $\tilde{g}_l$ of 0.011 27 than our earlier estimate because the correction term on the right-hand side of Eq. (21) is comparatively small. If this determination of the value for γ is valid, we can use it to derive a value for A_D from that of the experimentally determined parameter $\tilde{A}_D$ by use of Eq. (19). In this case, the value for A_D is 19.847 MHz, compared with $\tilde{A}_D=12.052$ MHz. A detailed description of the contact transformation of the Zeeman Hamiltonian is given in the Appendix.

In this paper we have described the detection of the fine-structure transition $^2\Pi_{1/2}\leftarrow{}^2\Pi_{3/2}$ in the FO radical by far-infrared laser magnetic resonance. The spin–orbit constant A_0, all four magnetic hyperfine parameters a, b_F, c, d, and a full set of g factors have been determined for the first time. The recorded data form the most accurate measurements on FO to date. Given sufficient sensitivity, it should be possible to detect magnetic dipole, pure rotational transitions in the microwave region. The predicted frequencies are given in Table VI. We intend to make these observations in the near future.

ACKNOWLEDGMENTS

This work supported in part by NASA Contract No. W-19, 167. We thank J. B. Burkholder for providing the ozone used for the experiment and L. R. Zink for helping with the measurements of the FIR laser lines. F.T. thanks the European Community, TMR Programme, for his fellowship (Contract No. ERBFMBICT950167).

TABLE VI. Predicted magnetic dipole rotational transitions of FO in the $^2\Pi_{3/2}$ spin state.

J'	F'	←	J	F	p	ν (MHz)
5/2	3		3/2	2	+	156 827.1
5/2	3		3/2	2	−	156 828.1
5/2	2		3/2	1	+	157 019.5
5/2	2		3/2	1	−	157 020.1
7/2	4		5/2	3	+	219 598.4
7/2	4		5/2	3	−	219 595.8
7/2	3		5/2	2	+	219 686.7
7/2	3		5/2	2	−	219 684.7
9/2	5		7/2	4	+	282 339.4
9/2	5		7/2	4	−	282 345.0
9/2	4		7/2	3	+	282 390.9
9/2	4		7/2	3	−	282 395.3
11/2	6		9/2	5	+	345 073.6
11/2	6		9/2	5	−	345 063.6
11/2	5		9/2	4	+	345 105.6
11/2	5		9/2	4	−	345 097.2
13/2	7		11/2	6	+	407 768.1
13/2	7		11/2	6	−	407 784.5
13/2	6		11/2	5	+	407 791.8
13/2	6		11/2	5	−	407 806.0
15/2	8		13/2	7	+	470 476.0
15/2	8		13/2	7	−	470 450.9
15/2	7		13/2	6	+	470 490.8
15/2	7		13/2	6	−	470 468.8

APPENDIX: TRANSFORMATION OF THE ZEEMAN AND MAGNETIC HYPERFINE STRUCTURE HAMILTONIANS

In a previous paper,[26] Brown and Watson transformed the spin–orbit Hamiltonian and demonstrated that γ and A_D are totally correlated for a molecule in a $^2\Pi$ state. In this section, we will apply the same contact transformation to the Zeeman and magnetic hyperfine structure Hamiltonians.

Generally speaking, the procedure consists of calculating an effective Hamiltonian $\tilde{H}$ from an original operator H through a unitary transformation of the form

$$\tilde{H}=e^{iU}He^{-iU}=H+i[U,H]+\cdots, \tag{A1}$$

where U is a suitable operator. The appropriate choice for U is $\theta\{L_z(J_xS_y-J_yS_x)\}$ where θ is a parameter which will be defined later.

For the moment let us consider just the Zeeman Hamiltonian, which has the form

$$H_Z=g_L\mu_BB_0L_Z+g_S\mu_BB_0S_Z-g_r\mu_BB_0N_Z + g_l\mu_B(S_xB_x+S_yB_y), \tag{A2}$$

where the smaller terms, depending on g_N, g_r' and g_l' have not been included [see Eq. (10)]. The calculation of the commutator $[U,H_Z]$ gives five terms:

$$\text{(i)}\quad i\mu_BB_0\theta g_L(\Phi_{Zx}S_x+\Phi_{Zy}S_y)L_z^2, \tag{A3}$$

$$\text{(ii)}\quad -i\mu_BB_0\theta\{g_S[\Phi_{Zx}(J_x-S_x)+\Phi_{Zy}(J_y-S_y)] + (g_l+g_r)(\Phi_{Zx}J_x+\Phi_{Zy}J_y)\}L_zS_z, \tag{A4}$$

$$\text{(iii)}\quad i\mu_BB_0\theta(g_S+g_r)\Phi_{Zz}L_z(\mathbf{J}\cdot\mathbf{S}-J_zS_z), \tag{A5}$$

$$\text{(iv)}\quad -i\mu_BB_0\theta(g_S+g_l+g_r)\Phi_{Zz}L_z(\mathbf{S}^2-S_z^2), \tag{A6}$$

$$\text{(v)}\quad i\mu_BB_0\theta g_r(\Phi_{Zx}S_x+\Phi_{Zy}S_y)L_zJ_z, \tag{A7}$$

where Φ_{Ff} is a direction cosine. Terms (i) and (iii) are contributions to g_l and give rise only to matrix elements off-diagonal in Ω and Σ. The expectation value of term (ii) is zero when calculated over the Hermitian average. Term (iv) is a contribution to g_L and term (v) is not considered because it is negligible. For a $^2\Lambda$ state, the matrix elements of term (i) diagonal in J and M_J and off-diagonal in Ω are of the form

$$i\mu_BB_0\theta g_L\Lambda^2M_J\frac{[(J-\Omega)(J+\Omega+1)]^{1/2}}{2J(J+1)}, \tag{A8}$$

where the corresponding matrix elements of term (iii) are

$$i\mu_BB_0\theta g_S\Lambda^2M_J\frac{[(J-\Omega)(J+\Omega+1)]^{1/2}}{2J(J+1)}. \tag{A9}$$

Brown and Watson showed[26] that, if A_D is fitted and γ is constrained to zero, the transformation parameter θ should be set equal to $\gamma/[(A-2B)\Lambda^2]$. Substituting these matrix elements in Eq. (A1), we obtain the effective values for $\tilde{g}_l$ and $\tilde{g}_L$,

$$\tilde{g}_l=g_l-\frac{\gamma}{(A-2B)}(g_L+g_S), \tag{A10}$$

$$\tilde{g}_L=g_L+\frac{\gamma}{2(A-2B)\Lambda^2}(g_S+g_l+g_r). \tag{A11}$$

The same transformation also modifies the nuclear hyperfine Hamiltonian. The untransformed hyperfine Hamiltonian is given by

$$H_{\text{hfs}}=aI_zL_z+b(I_xS_x+I_yS_y)+(b+c)I_zS_z + \tfrac{1}{2}d(e^{-2i\phi}I_+S_++e^{2i\phi}I_-S_-). \tag{A12}$$

The first term does not contribute to the transformed Hamiltonian because it commutes with U. The second and fourth terms have zero matrix elements when the Hermitian average is taken. The third term is the only one which needs to be calculated. The evaluation of the commutator gives

$$[U,(b+c)I_zS_z]=i\theta(b+c)(\mathbf{J}\cdot\mathbf{S}-J_zS_z)L_zI_z \tag{A13}$$

and the matrix elements diagonal in J, M_J, and M_I, and off-diagonal in Ω are

$$i\theta(b+c)\Lambda^2\frac{[(J-\Omega)(J+\Omega+1)]^{1/2}}{2J(J+1)}M_JM_I. \tag{A14}$$

Substituting $\theta=\gamma/[(A-2B)\Lambda^2]$ we obtain

$$-\frac{\gamma}{(A-2B)}(b+c)\frac{[(J-\Omega)(J+\Omega+1)]^{1/2}}{2J(J+1)}M_JM_I. \tag{A15}$$

The magnetic hyperfine matrix elements off-diagonal in Ω and diagonal in J, M_J, and M_I are

$$\left(b_F-\frac{c}{3}\right)\frac{[(J-\Omega)(J+\Omega+1)]^{1/2}}{2J(J+1)}M_JM_I. \tag{A16}$$

Since $b_F-c/3=b$ we can finally write the effective hyperfine parameter

$$\tilde{b}=b-\frac{\gamma}{(A-2B)}(b+c), \tag{A17}$$

where γ is constrained to zero in the fit. The parameter determined in a fit of data which show nuclear hyperfine structure is $\tilde{b}$, not b. Care must therefore be taken in the interpretation of such parameters in terms of the electronic structure of the molecule.

Similar modifications of nuclear hyperfine parameters have been described by Adam *et al.*[27] However, their effects arise from mixing with different (but nearby) electronic states whereas that given in Eq. (A17) arises entirely within the $^{2S+1}\Lambda$ state, from the procedure adopted to fit the experimental measurements.

[1] A. R. W. McKellar, Can. J. Phys. **57**, 2106 (1979).
[2] A. R. W. McKellar, C. Yamada, and E. Hirota, J. Mol. Spectrosc. **97**, 425 (1983).
[3] J. B. Burkholder, P. D. Hammer, C. J. Howard, and A. R. W. McKellar, J. Mol. Spectrosc. **118**, 471 (1986).
[4] P. D. Hammer, A. Sinha, J. B. Burkholder, and C. J. Howard, J. Mol. Spectrosc. **129**, 99 (1988).
[5] J. M. Brown, A. R. H. Cole, and F. R. Honey, Mol. Phys. **23**, 287 (1972).
[6] J. M. Brown, A. Carrington, and T. J. Sears, Mol. Phys. **37**, 1837 (1979).
[7] A. R. W. McKellar, J. Mol. Spectrosc. **86**, 43 (1981).
[8] A. R. W. McKellar, J. Mol. Spectrosc. **101**, 186 (1983).
[9] S. R. Langhoff, C. W. Bauschlicher Jr., and H. Partridge, Chem. Phys. Lett. **102**, 292 (1983).
[10] R. J. Saykally, K. G. Lubic, A. Scalabrin, and K. M. Evenson, J. Chem. Phys. **77**, 58 (1982).
[11] J. M. Brown, L. R. Zink, and K. M. Evenson, Phys. Rev. A **57**, 2507 (1998).
[12] E. C. C. Vasconcellos, S. C. Zerbetto, L. R. Zink, K. M. Evenson, R. M. Lees, and L.-X. Xu, J. Mol. Spectrosc. **188**, 102 (1988).
[13] M. Mizushima, K. M. Evenson, and J. S. Wells, Phys. Rev. A **5**, 2276 (1972).
[14] S. Saito, Y. Endo, M. Takami, and E. Hirota, J. Chem. Phys. **78**, 116 (1983).
[15] J. M. Brown, E. A. Colbourn, J. K. G. Watson, and F. D. Wayne, J. Mol. Spectrosc. **74**, 294 (1979).
[16] J. M. Brown, M. Kaise, C. M. L. Kerr, and D. J. Milton, Mol. Phys. **36**, 553 (1978).
[17] K. D. Hensel, R. A. Hughes, and J. M. Brown, J. Chem. Soc., Faraday Trans. **91**, 2999 (1995).
[18] J. M. Brown, C. R. Byfleet, B. J. Howard, and D. K. Russell, Mol. Phys. **23**, 457 (1972).
[19] R. N. Dixon and H. W. Kroto, Trans. Faraday Soc. **59**, 1484 (1963).
[20] T. C. Steimle, W.-L. Chang, D. F. Nachman, and J. M. Brown, J. Chem. Phys. **89**, 7172 (1988).
[21] J. M. Brown, J. E. Schubert, R. J. Saykally, and K. M. Evenson, J. Mol. Spectrosc. **120**, 421 (1986).
[22] J. S. M. Harvey, Proc. R. Soc. London, Ser. A **285**, 581 (1965).
[23] K. M. Evenson, R. J. Saykally, D. A. Jennings, R. F. Curl Jr., and J. M. Brown, *Chemical and Biochemical Applications of Lasers*, edited by C. B. Moore (Academic, New York, 1980), Vol. 5, pp. 95–138.
[24] A. Abragam and J. H. Van Vleck, Phys. Rev. **92**, 1448 (1953).
[25] L. Veseth, J. Mol. Spectrosc. **66**, 259 (1977).
[26] J. M. Brown and J. K. G. Watson, J. Mol. Spectrosc. **65**, 65 (1977).
[27] A. G. Adam, Y. Azuma, J. A. Barry, A. J. Merer, U. Sassenberg, J. O. Schröder, G. Cheval, and J. L. Féménias, J. Chem. Phys. **100**, 6240 (1994).
[28] N. G. Douglas, *Millimetre and Submillimetre Wavelength Lasers*, Springer Series in Optical Sciences Vol. 61 (Springer, New York, 1989).